

Ideal kink instability of a magnetic loop equilibrium

T. Török^{1,2}, B. Kliem¹, and V. S. Titov³

¹ Astrophysikalisches Institut Potsdam, 14482 Potsdam, Germany

² School of Mathematics and Statistics, University of St Andrews, St Andrews, Fife KY16 9SS, UK

³ Theoretische Physik IV, Ruhr-Universität Bochum, 44780 Bochum, Germany

Received 25 September 2003 / Accepted 3 November 2003

Abstract. The force-free coronal loop model by Titov & Démoulin (1999) is found to be unstable with respect to the ideal kink mode, which suggests this instability as a mechanism for the initiation of flares. The long-wavelength ($m=1$) mode grows for average twists $\Phi \gtrsim 3.5\pi$ (at a loop aspect ratio of ≈ 5). The threshold of instability increases with increasing major loop radius, primarily because the aspect ratio then also increases. Numerically obtained equilibria at subcritical twist are very close to the approximate analytical equilibrium; they do not show indications of sigmoidal shape. The growth of kink perturbations is eventually slowed down by the surrounding potential field, which varies only slowly with radius in the model. With this field a global eruption is not obtained in the ideal MHD limit. Kink perturbations with a rising loop apex lead to the formation of a vertical current sheet below the apex, which does not occur in the cylindrical approximation.

Key words. Instabilities – Magnetic fields – MHD – Sun: activity – Sun: corona – Stars: coronae

1. Introduction

Magnetic loops are the elementary building block of the solar corona and of low-plasma-beta environments of astrophysical objects in general. Understanding their instabilities is one of the fundamental problems in corona physics. Due to the small plasma beta ($\beta = P_{\text{kin}}/P_{\text{mag}} \sim 10^{-3} \dots 10^{-2}$ in the inner solar corona), the magnetic configuration of stable loops must be nearly force free. Any instability must be caused by currents flowing mainly along the loops. A sigmoidal (S- or inverse-S) shape of the projection of loops onto the solar surface is regarded as a signature of such currents, and indeed, a strong sigmoidal shape of soft X-ray loops correlates with eruptive activity (Canfield et al., 1999).

The stability of current-carrying force-free (or nearly force-free) fields was extensively studied for toroidal geometry in fusion research (see, e.g., Biskamp, 1993) and for cylindrical geometry with fixed ends in the astrophysical context. The latter is considered as an approximation to coronal loops with large aspect ratio which includes the effect of photospheric line tying (e.g., Hood & Priest, 1981; Velli et al., 1990; Mikić et al., 1990; Einaudi, 1990; Hood, 1992; Baty & Heyvaerts, 1996; Baty, 2001; Gerrard et al., 2002). It was found that the stability is mainly controlled by the total twist,

$$\Phi = \frac{lB_\phi(r)}{rB_z(r)}, \quad (1)$$

where l is the length of the current-carrying flux system, r is the (minor) radius, and B_z and B_ϕ are the axial and azimuthal field

components, respectively. In addition, the radial profile of the twist, the effect of line tying, and the ratio of radius and twist scale length ($\lambda = 2\pi l/\Phi$) are important. For example, the uniformly twisted force-free toroidal or periodic cylindrical configuration is kink-unstable for $\Phi > \Phi_c = 2\pi$, but line tying raises the instability threshold to $\approx 2.5\pi$ (Hood & Priest, 1981; Einaudi & Van Hoven, 1983). Localizing the current within a certain radius, a , and embedding it in a potential field also raises the threshold (as any substantial radial variation of the twist). Configurations of this type were found to be stable for $\Phi_{\text{max}} \lesssim 5\pi$, where Φ_{max} is the peak value of the twist in the configuration (Mikić et al., 1990; Baty & Heyvaerts, 1996). The instability threshold of embedded loops rises strongly if their radius becomes very small, i.e. if $\delta = 2\pi a/\lambda \lesssim 1$ (Baty, 2001). For cylindrical line-tied force-free configurations it was also shown that the longest-wavelength kink mode (azimuthal wave number $m=1$) becomes unstable before any other mode in the ideal MHD limit (Van der Linden & Hood, 1999).

The stability of arched magnetic loops has not yet been investigated. However, numerical studies of the injection of twist by slow vortex motions at the footpoints of an initially current-free loop-shaped flux bundle indicate that raising the twist of a loop beyond a critical value leads to destabilization (Amari et al., 1996; Török & Kliem, 2003). The critical twist lies in the range $2.5\pi < \Phi_c < 2.75\pi$ for the specific initial configurations studied. The driving by photospheric vortices generally influences a large surrounding volume in addition to the twisted loop. It also causes an increase of the loop length and width with increasing twist. Clearly, a stability consideration of loops free from such additional influences is needed.

Send offprint requests to: T. Török, e-mail: ttoeroek@aip.de

arXiv:astro-ph/0311198v1 9 Nov 2003

In this paper we study the stability of the loop model by Titov & Démoulin (1999), cited as T&D in the following (see their Fig. 2 for a schematic). This approximate, cylindrically symmetric, force-free equilibrium consists of a toroidal ring current of major radius R and minor radius a , whose outward-directed Lorentz self-force is balanced with the help of a field by two fictitious magnetic charges of opposite sign which are placed at the symmetry axis of the torus at distances $\pm L$ to the torus plane. That axis lies below the photospheric plane $\{z=0\}$ at a depth d . The resulting field outside the torus is current-free and contains a concentric magnetic X line between the torus and its centre. A toroidal field component created by a fictitious line current running along the symmetry axis is added. Its strength controls the twist of the field in the torus, and it turns the X line into a hyperbolic flux tube (HFT; for a definition, see Titov et al., 2002). The existence of the HFT is generic to such force-free configurations with a net current. The accuracy of the obtained equilibrium improves with decreasing parameters a/R and a/L . Its section in the volume $\{z > 0\}$ is a model of a coronal magnetic loop.

T&D have investigated the stability of the torus with respect to global expansion (growing perturbations $\delta R > 0$) and found instability for sufficiently large radii, $R \gtrsim \sqrt{2}L$. Roussev et al. (2003) confirmed this recently by numerical simulations, which also suggested that the instability threshold lies near $5L$ and that the slow decrease of the surrounding toroidal field with distance from the generating line current leads to saturation of the instability and prevents the loop from erupting. In the following, we investigate the stability of the configuration with respect to ideal kink modes in dependence of the twist in its coronal part.

2. Numerical model

Using the force-free equilibrium by T&D as the initial condition, we integrate the compressible ideal MHD equations to study whether instabilities occur. Based on the small value of the plasma beta in the inner corona, we use the simplifying assumption $\beta = 0$ in most of our parametric study:

$$\partial_t \rho = -\nabla \cdot (\rho \mathbf{u}), \quad (2)$$

$$\rho \partial_t \mathbf{u} = -\rho (\mathbf{u} \cdot \nabla) \mathbf{u} + \mathbf{j} \times \mathbf{B} + \nabla \cdot \mathbf{T}, \quad (3)$$

$$\partial_t \mathbf{B} = \nabla \times (\mathbf{u} \times \mathbf{B}), \quad (4)$$

$$\mathbf{j} = \mu_0^{-1} \nabla \times \mathbf{B}. \quad (5)$$

Here \mathbf{T} denotes the viscous stress tensor ($T_{ij} = \rho \nu [\partial u_i / \partial x_j + \partial u_j / \partial x_i - (2/3) \delta_{ij} \nabla \cdot \mathbf{u}]$) and ν is the kinematic viscosity, included to facilitate relaxation toward equilibrium in the stable cases.

The condition $\beta = 0$ ensures that the numerically obtained stable equilibria are force free, and in the unstable regime it yields higher growth rates than the runs with $\beta > 0$. Hence, the threshold for onset of instability is correctly obtained. For a few parameter sets, growth rates were also determined with the pressure gradient term, $-\nabla p$, included in Eq. (3); a standard form of the energy equation and an adiabatic equation of state were then added to Eqs. (2-5), as e.g., in Kliem et al. (2000).

The equations are normalized in the usual manner (see, e.g., Török & Kliem, 2003) by quantities derived from a characteristic length, taken here to be L , and the magnetic field, $B_0(0, 0, R-d)$, and Alfvén velocity, $v_{a0}(0, 0, R-d)$, at the loop axis at $t=0$. The loop is chosen to lie in the plane $\{x=0\}$. The initial density distribution is specified such that the Alfvén velocity is uniform, $\rho_0 = B_0^2$, and in most cases the computation is started with the system at rest, $\mathbf{u}_0 = 0$.

A modified Lax-Wendroff scheme is used on a nonuniform Cartesian grid in a box $[-L_x, L_x] \times [0, L_y] \times [0, L_z]$ with minimum grid spacing at the origin and very slowly increasing grid spacing toward the upper, side, and back boundaries. $L_x = L_y = L_z/2 = 5$ and $\Delta x_{\min} = \Delta y_{\min} = \Delta z_{\min} = 0.02$ are used. Line symmetry with respect to the z axis is prescribed at the front boundary, $\{y=0\}$, in order to use the available computing resources efficiently for maximum resolution. This implies $u_{x,y}(0, 0, z) = 0$. The variables are held fixed at their initial values at all other boundaries except for the bottom, where the tangential magnetic field components are extrapolated onto the ghost points. This permits a weak evolution of the fields in the plane $\{z=0\}$ ($\mathbf{u}(t) = 0$ and $\rho(t) = \rho_0$ in $\{z < 0\}$), enhancing stability in comparison to a bottom boundary with fixed variables (i.e., permitting the use of small diffusion parameters). A test run with fixed magnetic field at the bottom boundary (at $R = 2.2$, $\Phi_{\text{loop}} = 4.9\pi$) gave qualitatively identical results with a reduction of the growth rate by only 4 percent. A small amount of artificial spatial smoothing, $1 - \sigma_\rho = 1 - \sigma_u = 0.005$, is applied to the variables ρ and \mathbf{u} , respectively, to stabilize the scheme in addition to the stabilization by the viscosity ($\nu = 0.05$); see Török & Kliem (2003) for a detailed description of the numerical tools.

3. Kink instability

We start with a parameter set that is very close to those used by T&D and yields a configuration with left-handed field line twist which is stable against both global expansion and kink modes. We choose $d = L = 1$ (50 Mm), $R = 2.2$, and the number of field line turns about the axis of the whole torus at its surface to be $N_t = 5$, the coronal part being $N_{\text{loop}} = 1.75$. The values of the currents and charges used by T&D and their equilibrium conditions then yield $a = 0.65$. (The larger R , the smaller the resulting a/R , so we have chosen a value of R not much smaller than the estimated stability limit of the global expansion mode). The resulting coronal loop is shown in Fig. 1.

The T&D equilibrium has the property that the radial variation of the twist becomes substantial for $N_t \gtrsim R/a$ (Fig. 2). The average twist of this configuration is found to be $\Phi_t = 6.0\pi$, the fraction in its coronal part being $\Phi_{\text{loop}} = 2.1\pi$ (Table 1). Figure 1 shows that the loop is stable for these parameters and relaxes to a numerically force-free configuration very close to the approximate analytical equilibrium. The fluid velocity at the loop apex oscillates about zero with monotonically decreasing amplitude ($< 9 \times 10^{-5}$ by $t=78$). The HFT collapses into a small vertical current sheet as the loop settles to the numerical equilibrium, causing its inner edge to bulge out slightly (both effects are very weak at higher Φ , as long as $\Phi_{\text{loop}} < \Phi_c$.)

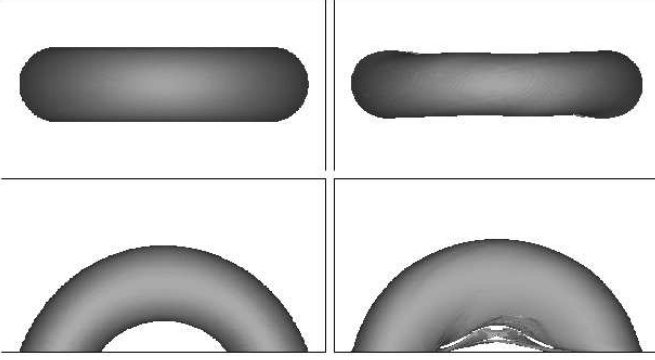


Fig. 1. Top and side view of the isosurface $|j| = 0.4 j_{\max}$ for $\Phi_{\text{loop}} = 2.1\pi$, $R = 2.2$, $\beta = 0$ at $t = 0$ (left) and $t = 78$ (right). Times are in units of τ_a . The volume $|x| \leq 1.5$, $|y| \leq 3$, $0 \leq z \leq 3$ is shown.

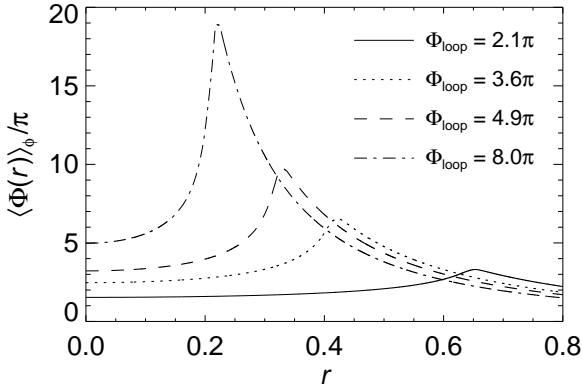


Fig. 2. Radial profile of the twist at the loop apex, averaged over azimuth angle ϕ ; $\langle \Phi(r) \rangle_\phi = (l/2\pi r) \int (B_\phi(r, \phi)/B_y(r, \phi)) d\phi$, $l = 2R \arccos(d/R)$, $r = (x^2 + (z - R + d)^2)^{1/2}$, $\phi = \arctan((z - R + d)/x)$; $\Phi_{\text{loop}} = (2/a^2) \int_0^a \langle \Phi(r) \rangle_\phi r dr$.

To check the stability of the loop, we have applied velocity perturbations uniform in direction with peak magnitude $u_1 = 0.05$ in a spherical volume with radius a and Gaussian profile at the loop apex, ramped up over 10 Alfvén times ($\tau_a = L/v_{a0}$) and then switched off. Both upward and downward directed perturbations were damped away within $\sim 20\tau_a$.

Next we consider the case $N_t = 15$ ($\Phi_{\text{loop}} = 4.9\pi$). This configuration shows the spontaneous development of the long-wavelength ($m=1$) kink mode very clearly (Figs. 3 and 4). The mode is initiated by the weak, downward-directed forces that result from the initial discretization errors of the current density on the grid. The figures also show a run with a small upward initial velocity perturbation applied at the apex ($u_1 = 0.01$, ramped up over $5\tau_a$); in this case the $m=1$ kink mode grows in a similar manner in the linear phase, with an azimuthal phase shift of π (opposite sigmoidal shape). Similar to the cylindrical case, the growth of the mode leads to the formation of a helically shaped current sheet at the interface of the perturbed loop with the surrounding magnetofluid. The upward directed kink instability of the loop forms a second, nearly vertical current sheet, at the HFT underneath, which does not occur in the cylindrical kink. The peak current density in these sheets rises

Table 1. Normalized parameters of the runs with $d=L=1$ and $\beta=0$, and growth rate of the kink instability for upward and downward apex motion. $\delta = (a/l)\Phi_{\text{loop}}$. Growth rates marked with a dag refer to runs with an initial velocity perturbation. The parameters of the first run correspond to the values given in Fig. 4 of T&D (except R).

R	N_t	a	Φ_{loop}/π	δ	$\gamma_{\text{up}} a/v_{a0}$	$\gamma_{\text{down}} a/v_{a0}$
2.2	5	0.65	2.1	0.88	0	0
2.2	9	0.44	3.3	0.96	0	0
2.2	10	0.42	3.6	0.98	0.008 [†]	0.001 [†]
2.2	12	0.37	4.2	1.00	0.031 [†]	0.023
2.2	15	0.32	4.9	1.03	0.059 [†]	0.052
2.2	20	0.27	6.0	1.06	0.088 [†]	0.076
2.2	25	0.24	7.0	1.08	0.102	0.091 [†]
2.2	30	0.21	8.0	1.10	0.111	0.100 [†]
3.4	9.1	0.44	5.0	0.80	0.005	
3.4	11.4	0.38	6.0	0.83	0.021	
3.4	13.9	0.34	7.0	0.87	0.034	
3.4	16.4	0.31	8.0	0.89	0.044	

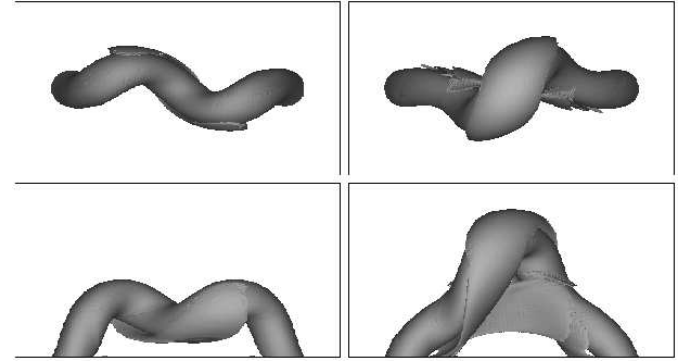


Fig. 3. Top and side view of current density isosurfaces for $\Phi_{\text{loop}} = 4.9\pi$, $R = 2.2$, $\beta = 0$. *Left:* $|j| = 0.15 j_{\max}$ at $t = 35$; unperturbed case. *Right:* $|j| = 0.25 j_{\max}$ at $t = 28$; run with an upward initial velocity perturbation at the loop apex; see the online edition for an animation of these data. $|x| \leq 1.5$, $|y| \leq 3$, $0 \leq z \leq 3$.

exponentially in the linear phase of the instability and exceeds that in the kinked loop in the nonlinear stage. The implications of the helical kinking and current sheet formation for the interpretation of sigmoidal structures in the solar corona have been discussed in Kliem et al. (2003). Figure 4 shows that the apex displacement grows exponentially: an instability occurs. The total kinetic energy in the box grows exponentially as well. Upward perturbations grow at a slightly higher rate because the restoring forces due to the toroidal field by the line current, the inertia of the fluid, and the effect of approach to a closed boundary are all weaker than for downward displacements. We expect that the kink mode with a sideward directed perturbation at the loop apex, which can in a first approximation be regarded as an azimuthally phase-shifted mode, is quantitatively similar to the modes with vertical perturbation at the apex studied here.

A fit of the growth rates for $R = 2.2$ suggests a critical average twist for onset of kink instability in the T&D equilibrium of $\Phi_c \approx 3.5\pi$, occurring at an aspect ratio of ≈ 5 (Fig. 5,

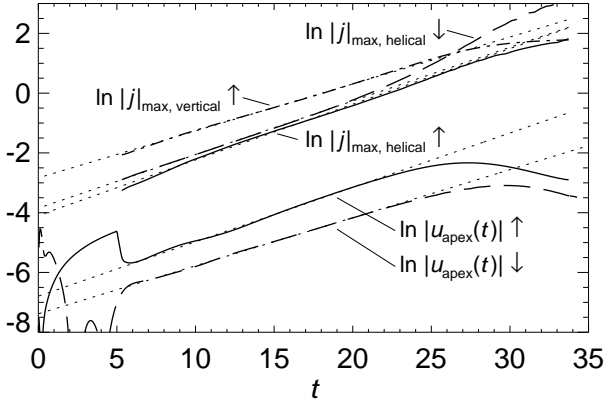


Fig. 4. Apex velocity and peak current density, $|j(0, 0, z, t)|_{\max}$, in the current sheets for upward (\uparrow) and downward (\downarrow) apex displacements. $R = 2.2$, $\Phi_{\text{loop}} = 4.9\pi$, $\beta = 0$. Exponential fits are shown dotted.

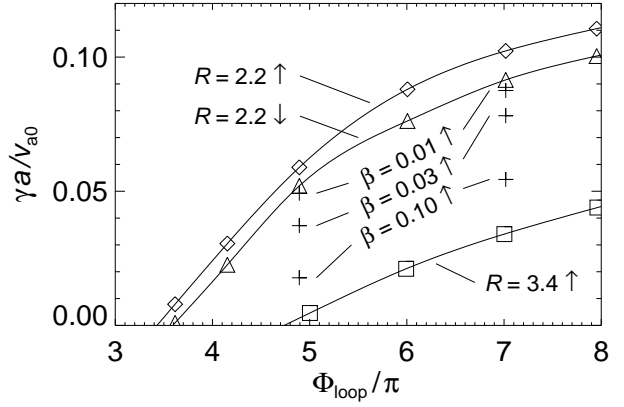


Fig. 5. Kink instability growth rates of the T&D equilibrium of radius R derived from the upward (\uparrow) and downward (\downarrow) apex velocities. Open symbols refer to runs with $\beta = 0$. $R = 2.2$ for all $\beta > 0$ runs.

Table 1). This threshold is similar to that found for cylindrical equilibria with similar twist profiles (e.g., Mikić et al., 1990; Baty & Heyvaerts, 1996). The growth rates, when normalized in the same manner ($\gamma a / v_{a0} [\Phi_{\text{loop}} - \Phi_c]$), are also similar (the factor $\approx 1/2$ in our growth rates nearly disappears if viscosities $\nu \lesssim 0.005$ are chosen; however, then the $m = 2$ mode starts to grow, which will be investigated separately).

A similar picture is obtained for larger loop radius R (and aspect ratio R/a). Since the parameter δ decreases with increasing R , the threshold of instability increases (Fig. 5). The threshold is probably smaller than $\approx 3.5\pi$ for $R < 2.2$, but the corresponding small aspect ratios are not characteristic of solar coronal loops. All growth rates are invariant against a reversal of the sign of the twist.

Runs with nonvanishing pressure (set uniform initially such that at the loop axis $\beta = 0.01$; 0.03 ; 0.1) show identical qualitative behaviour with reduced growth rates (Fig. 5).

The instability enters a nonlinear saturation phase in all runs. The apex velocity then drops, but the current density in the formed sheets continues to rise until numerical instability is unavoidable. Apparently, a global eruption is not reached in ideal-MHD simulations, due to the counteraction by the strong overlying field in the model, as also found by Roussev et al. However, the exponential rise and helical shape of the loop and the saturation correspond excellently to eruptive filaments that do not succeed to escape from the Sun (Ji et al., 2003).

Finally, we have checked whether the numerical equilibria develop a sigmoidal shape as the twist approaches Φ_c from below. No indication of sigmoidality could be found up to $\Phi_{\text{loop}} = 3.3\pi$ ($N_t = 9$). Even after applying an upward initial perturbation as in the run with $N_t = 5$, the loop relaxed to its original circular shape, straight in projection and similar to that shown in Fig. 1.

4. Conclusions

The magnetic loop equilibrium by Titov & Démoulin (1999) is kink-unstable for twists $\Phi > \Phi_c$, with $\Phi_c \approx 3.5\pi$ at a loop aspect ratio $R/a \approx 5$. The instability threshold rises with rising

aspect ratio. No indication of sigmoidal shape at slightly subcritical twists was found. The unstable kink mode with upward displacement of the loop apex forms a vertical current sheet at the HFT underneath the loop, which has no counterpart in kink-unstable cylindrical loop models but corresponds to the central element of the “standard flare model” (e.g., Shibata, 1999). The surrounding potential field eventually terminates the exponential growth of kink modes in the considered configuration, apparently inhibiting a global eruption within the framework of ideal MHD. However, the configuration may nevertheless suffer a global eruption if (a) a surrounding field which decreases more rapidly with height is employed, (b) magnetic reconnection is permitted to occur in the formed current sheets, or (c) magnetic reconnection with neighbouring loops is triggered in a multiple-loop configuration.

Acknowledgements. This investigation was supported by BMBF/DLR grants 50 OC 9901 2, and 01 OC 9706 4, by the Volkswagen Foundation, and by EU grant HPRN-CT-2000-00153. The John von Neumann-Institut für Computing, Jülich granted Cray computer time.

References

- Amari, T., Luciani, J. F., Aly, J. J., & Tagger, M. 1996, *ApJ*, 466, L39
- Baty, H. 2001, *A&A*, 367, 321
- Baty, H., & Heyvaerts, J. 1996, *A&A*, 308, 935
- Biskamp, D. 1993, *Nonlinear Magnetohydrodynamics*, (CUP)
- Canfield, R. C., Hudson, H. S., & McKenzie, D. E. 1999, *Geophys. Res. Lett.*, 26, 627
- Einaudi, G. 1990, in *Physics of Magnetic Flux Ropes*, ed. C. T. Russell, E. R. Priest, & L. C. Lee (AGU, Washington) 43
- Einaudi, G., & Van Hoven, G. 1983, *Sol. Phys.*, 88, 163
- Gerrard, C.L., Arber, T.D., & Hood, A.W. 2002, *A&A* 387, 687
- Hood, A. W. 1992, *Plasma Phys. & Contr. Fusion*, 34, 411
- Hood, A. W., & Priest, E. R. 1981, *Geophys. Astrophys. Fluid Dynamics*, 17, 297
- Ji, H., et al. 2003, *ApJ*, 595, L135
- Kliem, B., Karlický, M., & Benz, A. O. 2000, *A&A*, 360, 715
- Kliem, B., Titov, V. S., & Török, T. 2003, *A&A*, in press

- Mikić, Z., Schnack, D.D., & VanHoven, G. 1990, ApJ 361, 690
- Roussev, I. I., et al. 2003, ApJ, 588, L45
- Shibata, K. 1999, Ap&SS, 264, 129
- Titov, V. S., & Démoulin, P. 1999, A&A, 351, 707 (T&D)
- Titov, V. S., Hornig, G., & Démoulin, P. 2002, J. Geophys. Res., 107, doi:10.1029/2001JA000278
- Török, T., & Kliem, B. 2003, A&A, 406, 1043
- Van der Linden, R.A.M., & Hood, A. W. 1999, A&A, 346, 303
- Velli, M., Einaudi, G., & Hood, A. W. 1990, ApJ, 350, 428